Initial State Helicity Correlation in Wide Angle Compton Scattering

(A Proposal to Jefferson Lab (PAC 42))

D. Nikolenko, I. Rachek, Yu. Shestakov
Budker Institute, Novosibirsk, Russia

G.B. Franklin, V. Mamyan, B. Quinn
Carnegie Mellon University, Pittsburgh, PA 15213

T. Averett, C. Perdrisat, H. Yao
College of William and Mary, Williamsburg, VA 23185

E. Christy, N. Kalantarians, M. Kohl
Hampton University, Hampton, VA 23668

S. Širca, J. Beričič, M. Mihovilovič, S. Štajner
J. Stefan Institute and Dept. of Physics, University of Ljubljana, Slovenia

W. Boeglin, P. Markowitz
Florida International University, Miami, FL 33199

J. Dunne, D. Dutta, M.H. Shabestari, L. Ye
Mississippi State University, Mississippi State, MS 39762

V. Punjabi
Norfolk State University, Norfolk, VA 23504

A. Ahmidouch, S. Danagoulian
North Carolina A&T State University, Greensboro, NC 27411

I. Albayrak, M. A. Pannunzio Carmignotto, J. Denes-Couto,
N. Hlavin, B. Nepal
North Carolina Central University, Durham, NC 27707

M. Amaryan, G. Dodge, L. El Fassi, C. Hyde-Wright, A. Radyushkin,
L. Weinstein
Old Dominion University

R. Gilman, K. Myers, R. Ransome
Rutgers, The State University of New Jersey, Piscataway, NJ 08854

E. Piasetzky, G. Ron
Tel Aviv University, Israel

A. Lukhanin, Z.-E. Meziani
Temple University, Philadelphia, PA 19122

I. Albayrak, T. Horn, F. Klein
The Catholic University of America, Washington DC, 20064

A. Camsonne, J. P. Chen, E. Chudakov, J. Gomez, D. Gaskell, O. Hansen,
D. W. Higinbotham, M. Jones, C. Keppel, D. Mack, R. Michaels, B. Sawatzky,
G. Smith, S. Wood
Thomas Jefferson National Accelerator Facility, Newport News, VA 23606

D. J. Hamilton, J. R. M. Annand, D. I. Glazier, D. G. Ireland,
I. J. D. MacGregor, B. McKinnon, B. Seitz, D. Sokhan
University of Glasgow, Glasgow, Scotland

T. Badman, E. Long, K. Slifer, P. Solvignon, R. Zielinski
University of New Hampshire, Durham, NH 03824

G. Cates, D. Crabb, **D. Day** (spokesperson), N. Dien,
C. Gu, **D. Keller**(spokesperson, contact), R. Lindgren, J. Liu,
N. Liyanage, V. Nelyubin, P. Peng, O. Rondon,
J. Zhang(spokesperson)
University of Virginia, Charlottesville, VA 22904

A. Asaturyan, A. Mkrtchyan, H. Mkrtchyan, A. Shahinyan, V. Tadevosyan,
H. Voskanyan, S. Zhamkochyan
A. I. Alikhanyan National Science Laboratory (Yerevan Physics Institute), Yerevan 0036,

The Neutral Particle Spectrometer collaboration
`https://wiki.jlab.org/cuawiki/index.php/Collaboration`

May 29, 2014

Contents

Abstract

We propose an experiment to measure the initial state helicity correlation asymmetry A_{LL} in Real Compton Scattering (RCS) by scattering longitudinally polarized photons from a longitudinally polarized proton target at the invariant s= 8 (GeV/c)^{2}for three scattering angles, $\theta_\gamma^{cm} = 60°$, 90° and 136°.

The recent JLab RCS experiment, E99-114 and E07-002, demonstrated the feasibility of the experimental technique. The experiment utilizes an untagged bremsstrahlung photon beam and the UVA polarized target. The scattered photon is detected in the future Neutral Particle Spectrometer (NPS). The coincident recoil proton is detected in the Hall C magnetic spectrometer HMS.

The applicability of QCD ,in the moderate energy range, to exclusive reactions is a subject of great interest and any opportunity to test unambiguously its prediction should be taken.

Recent calculations by G. A. Miller in a constituent quark model reproduced the K_{LL} experimental result but revealed a large disagreement with the GPD prediction for A_{LL}. It is but one of the goals of our proposal to test this prediction which could force a modification of our understanding of the high-t photo-induced processes like RCS, pion photoproduction, and deuteron photo–disintegration. A measure of $A_{LL}$and the conclusions that can be drawn from the results would give insight into understanding quark orbital angular momentum in the proton.

We request 742 hours of 90 nA at 4.4 GeV electron beam to measure the polarization observable A_{LL} to a statistical accuracy better than 0.07. This measurement will significantly increase our experimental confidence in the application of the GPD approach to reactions induced by real photons which play a major role in nucleon structure physics in the JLab energy range.

1 Introduction

Significant progress has been made over the last decade in our understanding of exclusive reactions in the hard scattering regime. This progress had been made possible (in part) by data from Jefferson Lab on elastic electron scattering and Compton scattering from the proton and by a significant and increasingly sophisticated theoretical effort to exploit the richness of exclusive reactions at moderate momentum transfers.

The observation of scaling in Deep Inelastic Scattering (DIS) at relatively low momentum transfers, successfully understood within the framework of pQCD, suggested that the same interpretation would be fruitful when applied to exclusive reactions: elastic electron scattering, photo- and electro-production of mesons, and Compton scattering. This prospect was further supported by the fact that constituent counting rules [1, 2], which naturally govern reactions that conform to the pQCD picture, could describe certain exclusive reactions.

There is little doubt that the pQCD mechanism dominates at high energies. What has been lacking is a general agreement as to how high the energy must be for pQCD to be completely applicable. The argument on this point is driven by more than a difference of (theoretical) opinion. The unavoidable fact is that cross sections calculated in a pQCD framework have invariably been low when compared to data, sometimes by an order of magnitude or more[3].

Results of two experiments at Jefferson Lab on the proton contradict the predictions of pQCD: the recoil polarization measurements of G_E^p E93-027 and E99-007, and the Real Compton Scattering (RCS) experiment E99-114. The G_E^p measurements[4, 5] found that the ratio of F_2 and F_1, scaled by Q^2 demands a revision of one of the precepts of pQCD, namely hadron helicity conservation. Results from the RCS measurement[6] are that the longitudinal polarization transfer K_{LL} is large and positive, also contrary to the pQCD predictions which find K_{LL} to be small and negative. These two experiments provide a compelling argument that pQCD should not be applied to exclusive processes at energy scales of 5-10 GeV.

Fortunately, an alternate theoretical framework exists [7, 8, 9] for the interpretation of exclusive scattering at intermediate energies. This alternative approach asserts the dominance of the handbag diagram in which the reaction amplitude factorizes into a subprocess involving a hard interaction with a *single quark*. The coupling of the struck quark to the spectator system is described by the Generalized Parton Distributions (GPD's) [10, 11]. Since the GPD's are independent of the particular hard scattering reaction, the formalism leads to a unified description of hard exclusive reactions. Moreover, the relationship between GPD's and the normal parton distribution functions provides a natural framework for relating inclusive and exclusive reactions.

The RCS experiment E99-114 produced an especially remarkable result; not only was the measurement of K_{LL} inconsistent with pQCD, it was found that the longitudinal polarization is nearly as large as that expected for scattering from a free quark.

The QCD factorization approach formulated in the framework of SCET can be used to develop a description of the soft-spectator scattering contribution. Recently a derivation of the complete factorization for the leading power contribution in wide angle Compton scattering has been worked out in the soft collinear effective theory [12, 13]. As factorization evolves and becomes less dependent on the assumption of restricted parton virtualities and parton transverse momenta RCS should receive the same level of attention that DVCS has. RCS have a complementary nature to DVCS in so far as in DVCS the GPDs are probed at small t while for RCS (and nucleon form factors) the GPDs are probed at large t.

The initial state helicty correlation can be used to probe a theoretical model in detail. According to the handbag approach their angle dependence is close to that of the subprocess $\gamma q \to \gamma q$ diluted by form factors which take into account that the proton is a bound state of quarks and which represent $1/x$ moments of GPDs. The electromagnetic nucleon form factors have been revised using the generalized parton distributions analysis by M. Diehl and P. Kroll [14]. The various theoretical efforts made to apply the handbag approach to wide angle compton scattering (WACS) have produced predictions for its polarization observables including K_{LL} and A_{LL} [9, 15]. We must emphasize that the results of E99-114 are at a single kinematic point of a single observable. It is essential to verify the dominance of the handbag mechanism in other observables such as A_{LL}. In a recent development, a calculation of Miller suggests that a measurement of A_{LL} in WACS would be a test of perturbative chiral symmetry and of the mass of the quarks participating in the hard scattering.

There is much theoretical interest in WACS but a bit less activity at present which is only due to the lack of new data. The polarized observables are essential for moving the framework forward. There was only one polarization measurement of K_{LL} made during E99-114, so a similar experiment (E07-002) [16] at higher s was undertaken in Hall C to acquire three more K_{LL} points, the analysis of which is nearing completion. The next step is to obtain the K_{LL} compliment by measuring the initial state helicity correlation asymmetry A_{LL} using a polarized proton target. We therefore propose a measurement of the polarization observable A_{LL} in Compton scattering at an incident energy of 4.4 GeV.

The proposal is organized as follows. In Section 2 we describe in more detail the handbag formalism and the predictions for RCS, some results from E99-114, and a summary of the physics goals of the proposed experiment. In Section 3 we describe the experimental approach and both the standard and the specialized equipment. In subsequent sections, we present our proposed measurements (Sec. 4), our expected results and beam time request (Sec. 5). Finally, the proposal is summarized in Section 6.

2 Physics Motivation

2.1 Overview

In view of the remarks in the Introduction, we consider several interesting questions that motivate us to explore further the measurement of polarization observables in RCS at JLab:

1. What is the nature of the quark which absorbs and emits photons in the RCS process in the wide angle regime? Is it a constituent or a current quark?

2. If the GPD approach is correct, is it indeed true that the RCS reaction proceeds through the interaction of photons with a single quark?

3. What are the constraints on the GPD integrals imposed from the proposed measurement of the A_{LL} observable.

In order to present a framework for addressing these issues, we next briefly discuss WACS in the soft-collinear effective theory, the handbag mechanism in the GPD conceptualization, and the handbag mechanism in the constituent quark model.

2.2 Soft-collinear Effective Theory

Recently a complete factorization formula for the leading power contribution in wide angle Compton scattering has been developed [12, 13]. The soft-spectator contribution describes the scattering which involves the soft modes and resulting soft-spectator scattering contribution to the overall amplitude. The soft collinear effective theory is used in order to define this contribution in a field theoretical approach. The SCET framework is then used to provide a proof of the factorization formula.

The SCET framework permits the implementation of some specific corrections which are related to the soft-overlap contribution. There are indications that numerical effect of this contribution can be dominant at some moderate values of the Mandelstam variables. In general, SCET give a very solid description in the region where the other power corrections are small.

The SCET formalism follows the same idea as in the standard factorization approach, short and long distance physics are factorized separately. The only required assumptions are very general such as that soft partons have soft momenta of order Λ_{qcd}. There is not additional need to constrain the virtualities by hand. The advantage of SCET formalism is a systematic approach to the factorization of the hard and soft subprocesses.

The asymmetry K_{LL} is studied with the approximation that the hard-spectator contributions are small. Neglecting all power corrections and using the next-to-leading expressions some numerical results as a function of the scattering angle θ are obtained (see Fig.1). The solid red line corresponds to the leading-order approximation. The dashed (blue) and dotted (black) lines show the numerical results for the complete NLO expression for the energies $s = 6.9$ GeV^2 and $s = 20$ GeV^2, respectively. The data point is from E99-114 and corresponds to $s = 6.9$ GeV^2. The value of the longitudinal asymmetry K_{LL} is qualitatively different from the one that can be obtained in the hard-spectator (hard two-gluon exchange) factorization picture.

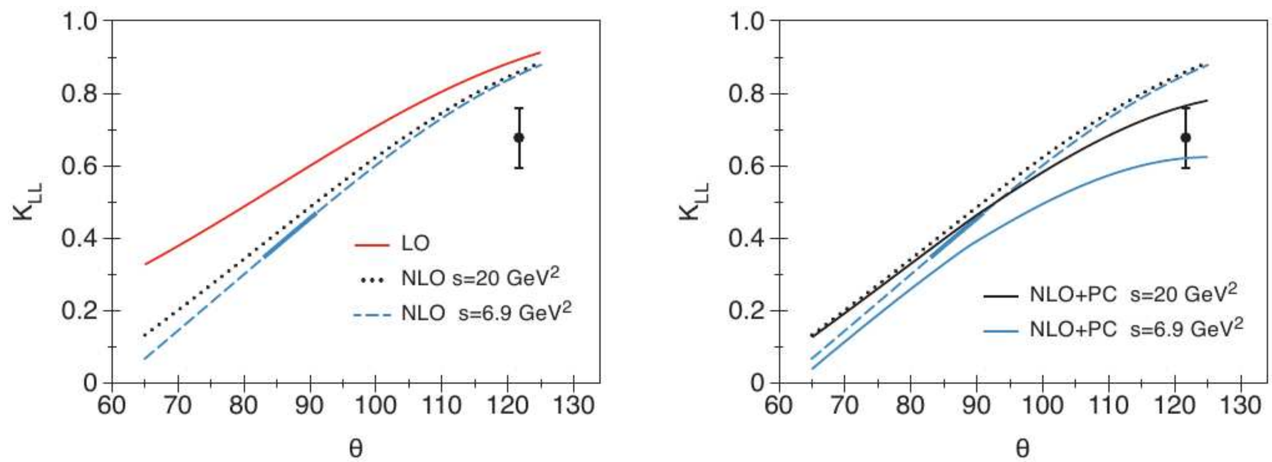

Figure 1: The longitudinal asymmetry K_{LL} as a function of scattering angle θ. (Left) A comparison of the LO (red) and NLO calculated with $s = 6.9$ GeV^2 (dashed) and $s = 20$ GeV^2 (dotted) lines. (Right) A comparison of the NLO results calculated with (solid black) and without (blue line) kinematical power corrections. The massless approximation is the same for both plots.

It is very relevant to describe a factorization for the helicity flip amplitudes but the modeling will be dependent on the new unknown nonperturbative matrix elements. Any experimental data on A_{LL} directly can provide the needed information to move forward in the acquisition of these nonperturbative quantities.

2.3 pQCD Mechanism

The traditional framework for the interpretation of hard exclusive reactions in the asymptotic regime is perturbative QCD (pQCD) [17, 18]. The onset of scaling in Deep Inelastic Scattering (DIS) at the relative low scale of $Q^2 \sim 1$–2 (GeV/c)^2, gives rise to the expectation that pQCD might also be applicable to exclusive processes in the range of a few (GeV/c)^2. pQCD confronts RCS [19, 20, 3] as shown in Fig. 2, where it is seen that the three valence quarks are active participants in the hard subprocess, which is mediated by the exchange of two hard gluons. The soft physics is contained in the valence quark distribution amplitudes. The pQCD mechanism leads naturally to the constituent counting rules for exclusive processes:

$$\frac{d\sigma}{dt} = \frac{f(\theta_{cm})}{s^n}, \tag{1}$$

where n is related to the number of active constituents in the reaction and $f(\theta_{cm})$ is a function only of the center of mass scattering angle[1, 2]. Indeed, the observation that many exclusive reactions, such as elastic electron scattering, pion photoproduction, and RCS, approximately obey Eq. 1 has led to the belief that the pQCD mechanism dominates at experimentally accessible energies. There seems to be little theoretical disagreement that the pQCD mechanism dominates at sufficiently high energies [17]; however, there is no consensus on how high is "sufficiently high." Despite the observed scaling, absolute cross sections calculated using the pQCD framework are very often low compared to existing experimental data, sometimes by more than an order of magnitude[3]. Moreover, several recent JLab experiments that measure polarization observables also disagree with the predictions of pQCD. In the G_E^p experiment [4, 5] the slow falloff of the Pauli form factor $F_2(Q^2)$ up to Q^2 of 5.6 (GeV/c)^2 provides direct evidence that hadron helicity is not conserved, contrary to predictions of pQCD. Similar findings were made in the π^0 photoproduction experiment [21], where both the non-zero transverse and normal components of polarization of the recoil proton are indicative of hadron helicity-flip, which is again contrary to the predictions of pQCD. Finally, in the recently completed RCS experiment, E99-114, the longitudinal polarization transfer K_{LL} (which will be defined precisely in the next section) shows a value which is large and positive, contrary to the pQCD prediction which is small and negative [3]. For all these reasons, it can be argued that pQCD is not the correct mechanism for interpreting exclusive reactions at currently accessible energies and instead we should seek a description in terms of the handbag mechanism.

pQCD calculations predict that A_{LL}=K_{LL}, so a measurement of A_{LL} in combination with the already obtained result for K_{LL} could provide an additional test of pQCD applicability in the JLab energy regime.

2.4 Handbag Mechanism

The handbag mechanism offers new possibilities for the interpretation of hard exclusive reactions. For example, it provides the framework for the interpretation of deep exclusive reactions, which are reactions initiated by a high-Q^2 virtual photon. The application of the formalism to RCS (see Fig. 3) was initially worked out to leading order (LO) by Radyushkin [7] and subsequently by Diehl *et al.*[8]. More recently next-to-leading-order (NLO) contributions have been worked out by Huang *et al.*[9]. The corresponding diagram for elastic electron scattering is similar to Fig. 3, except that there is only one external virtual photon rather than two real photons. In the handbag approach, the hard physics is contained in

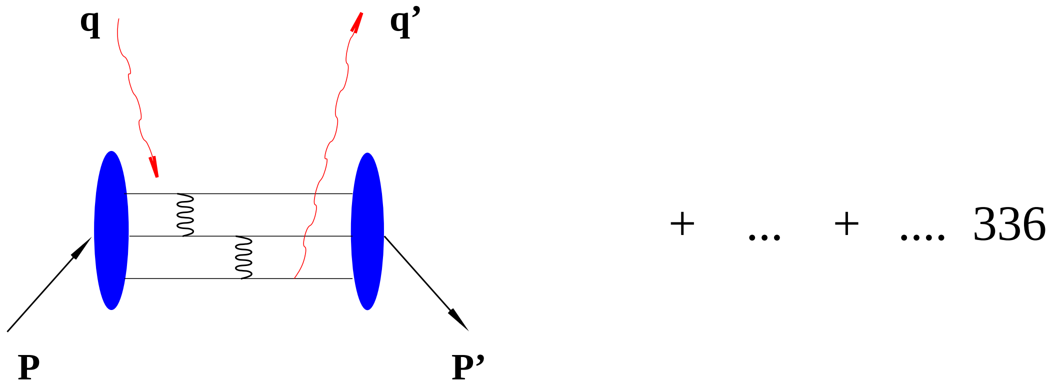

Figure 2: Two gluon exchange pQCD diagram for RCS. 336 diagrams can contribute.

the scattering from a single active quark and is calculable using pQCD and QED: it is just Compton scattering from a structureless spin-1/2 particle.

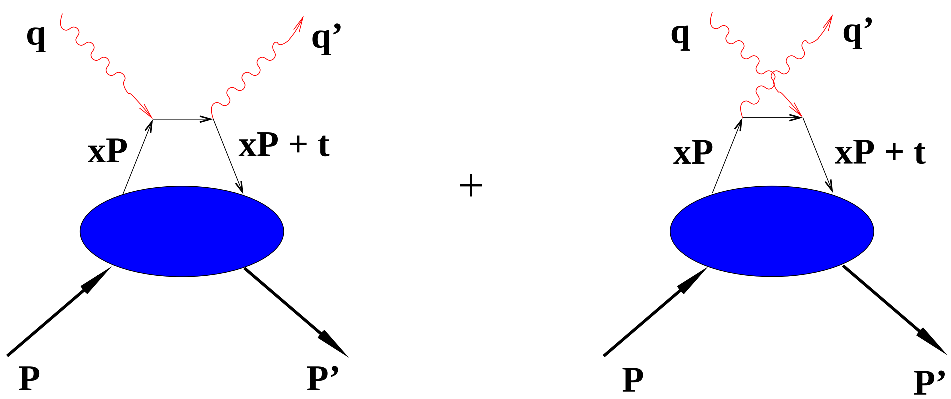

Figure 3: The handbag diagram for RCS.

The soft physics is contained in the wave function describing how the active quark couples to the proton. This coupling is described in terms of GPD's. The GPD's have been the subject of intense experimental and theoretical activity in recent years [10, 11]. They represent "superstructures" of the proton, from which are derived other measurable structure functions, such as parton distribution functions (PDF) and form factors (F_1 and F_2). To NLO, only three of the four GPD's contribute to the RCS process: $H(x, \xi = 0, t)$, $\hat{H}(x, \xi = 0, t)$, and $E(x, \xi = 0, t)$. Since the photons are both real, the skewness parameter ξ is zero, reflecting the fact that the momentum absorbed by the struck quark is purely transverse. In the handbag formalism, the RCS observables are new form factors of the proton that are

x^{-1}-moments of the GPD's:

$$\begin{aligned}
R_{\scriptscriptstyle V}(t) &= \sum_a e_a^2 \int_{-1}^{1} \frac{dx}{x} H^a(x,0,t), \\
R_{\scriptscriptstyle A}(t) &= \sum_a e_a^2 \int_{-1}^{1} \frac{dx}{x} \,\mathrm{sign}(x)\, \hat{H}^a(x,0,t), \\
R_{\scriptscriptstyle T}(t) &= \sum_a e_a^2 \int_{-1}^{1} \frac{dx}{x} E^a(x,0,t),
\end{aligned}$$

where e_a is the charge of the active quark and the three form factors are, respectively, the vector, axial vector, and tensor form factors. (sign(x) is the sign of x $\equiv \frac{x}{|x|}$.) The corresponding form factors for elastic electron or neutrino scattering are given by the first (x^0) moments of the same GPD's:

$$\begin{aligned}
F_{\scriptscriptstyle 1}(t) &= \sum_a e_a \int_{-1}^{1} dx\, H^a(x,0,t), \\
G_{\scriptscriptstyle A}(t) &= \sum_a \int_{-1}^{1} dx \,\mathrm{sign}(x)\, \hat{H}^a(x,0,t), \\
F_{\scriptscriptstyle 2}(t) &= \sum_a e_a \int_{-1}^{1} dx\, E^a(x,0,t),
\end{aligned}$$

where the three quantities are, respectively, the Dirac, axial, and Pauli form factors. On the other hand, the $t = 0$ limit of the GPD's produce the PDF's:

$$\begin{aligned}
H^a(x,0,0) &= q^a(x), \\
\hat{H}^a(x,0,0) &= \Delta q^a(x) \\
E^a(x,0,0) &= 2\frac{J^a(x)}{x} - q^a(x),
\end{aligned} \tag{2}$$

where J^a is the total angular momentum of a quark of flavor a and is not directly measurable in DIS.

In the handbag factorization scheme, the RCS helicity amplitudes are related to the form factors by

$$\begin{aligned}
M_{\mu'+,\mu+}(s,t) &= 2\pi\alpha_{em}\left[T_{\mu'+,\mu+}(s,t)(R_{\scriptscriptstyle V}(t) + R_{\scriptscriptstyle A}(t)) + T_{\mu'-,\mu-}(s,t)(R_{\scriptscriptstyle V}(t) - R_{\scriptscriptstyle A}(t))\right], \\
M_{\mu'-,\mu+}(s,t) &= 2\pi\alpha_{em}\frac{\sqrt{-t}}{m}\left[T_{\mu'+,\mu+}(s,t) + T_{\mu'-,\mu-}(s,t)\right] R_{\scriptscriptstyle T}(t),
\end{aligned}$$

where μ, μ' denote the helicity of the incoming and outgoing photons, respectively. The signs on M and T refer to the helicities of the proton and active quark, respectively. This structure of the helicity amplitudes leads to a simple interpretation of the RCS form factors: $R_V \pm R_A$ is the response of the proton to the emission and reabsorption of quarks with helicity in the same/opposite direction of the proton helicity, and R_T is directly related to the proton helicity-flip amplitude [9]. These equations leads to expressions relating RCS observables to the form factors.

The most important of these experimentally are the spin-averaged cross section and the recoil polarization observables. The spin-averaged cross section factorizes into a simple product of the Klein-Nishina (KN) cross section describing the hard scattering from a single quark, and a sum of form factors depending only on t [7, 8]:

$$\frac{d\sigma/dt}{d\sigma_{\mathrm{KN}}/dt} = f_V \left[R_V^2(t) + \frac{-t}{4m^2} R_T^2(t) \right] + (1 - f_V) R_A^2(t) \,, \tag{3}$$

For the interesting region of large $p_\perp$, the kinematic factor f_V is always close to 1. Consequently the unpolarized cross sections are largely insensitive to R_A, and the left-hand-side of Eq. 3 is nearly s-independent at fixed t. One of the primary goals of E99-114 was to test this relationship as well as to determine the vector form factor R_V. The recent calculations to NLO, which take into account both photon and proton helicity-flip amplitudes, do not change this prediction in any appreciable way [9, 22]. Updated cross section and Compton form factors (see Fig. 4) with their parametric uncertainties have also recently been evaluated [14].

The longitudinal and transverse polarization transfer observables, K_{LL} and K_{LS}, respectively, are defined by

$$K_{LL} \frac{d\sigma}{dt} \equiv \frac{1}{2} \left[\frac{d\sigma(\uparrow\uparrow)}{dt} - \frac{d\sigma((\downarrow\uparrow)}{dt} \right] \qquad K_{LS} \frac{d\sigma}{dt} \equiv \frac{1}{2} \left[\frac{d\sigma(\uparrow\rightarrow)}{dt} - \frac{d\sigma(\downarrow\rightarrow)}{dt} \right] \tag{4}$$

where the first arrow refers to the incident photon helicity and the second to the recoil proton helicity ($\uparrow$) or transverse polarization ($\rightarrow$).

With definitions of two additional parameters

$$\beta = \frac{2m}{\sqrt{s}} \frac{\sqrt{-t}}{\sqrt{s} + \sqrt{-u}} \qquad \kappa(t) = \frac{\sqrt{-t}}{2m} \frac{R_T(t)}{R_V(t)} \,, \tag{5}$$

the three polarization observables are approximately related to the form factors by the expressions [8, 9]

$$K_{LL} \approx K_{LL}^{\mathrm{KN}} \frac{R_A(t)}{R_V(t)} \frac{1 - \beta\kappa(t)}{1 + \kappa^2(t)} \qquad \frac{K_{LS}}{K_{LL}} \approx \kappa(t) \frac{1 + \beta\kappa^{-1}(t)}{1 - \beta\kappa(t)} \qquad P_N \approx 0 \,, \tag{6}$$

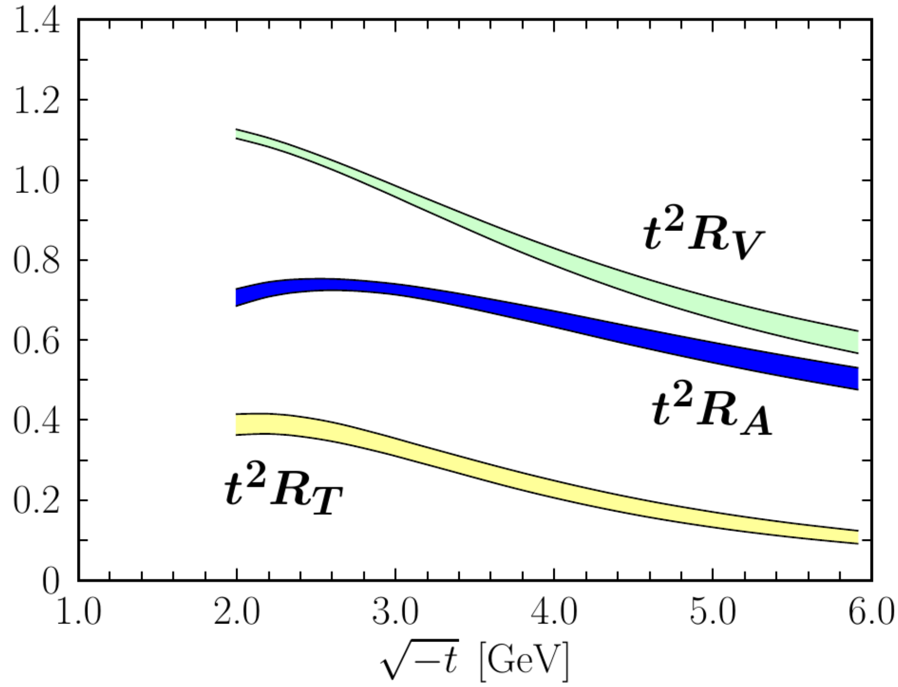

Figure 4: Predictions for the Compton form factors evaluated from the M. Diehl, P. Kroll default fit from Ref. [9], scaled by t^2 and shown in units of GeV^4. The bands in each case show the parametric uncertainties.

where K_{LL}^{KN} is the longitudinal asymmetry for a structureless Dirac particle. These formulas do not include small gluonic corrections, which are discussed in Ref. [9].

The expressions above show that measurements of K_{LL} and K_{LS}, when combined with measurements of $d\sigma/dt$ (*i.e.* from E99-114), allow determinations of all three form factors. They also show that two very important pieces of information follow directly from the spin asymmetries: K_{LL} and K_{LS} / K_{LL}, which are directly related to the form factor ratios R_A/R_V and R_T/R_V, respectively.

The initial state helicity correlation parameter is defined by,

$$A_{LL}\frac{d\sigma}{dt} \equiv \frac{1}{2}\left[\frac{d\sigma(\uparrow\uparrow)}{dt} - \frac{d\sigma((\downarrow\uparrow)}{dt}\right] \tag{7}$$

where the first arrow refers to the incident photon helicity and the second to the initial state proton helicity ($\uparrow$). In the GPD approach of Ref. [9], the initial state helicity correlation parameter, A_{LL}, equals K_{LL} so all the predicted relationships between A_{LL} and the RCS form factors are the same as shown above for K_{LL}.

From the relationships (Eq. 2) connecting the RCS form factors to PDFs, the ratio R_A/R_V is related to $\Delta q^a(x)/q^a(x)$. For RCS, the e_a^2-weighting of the quark flavors means that u quarks will dominate the reaction. Moreover, at relatively large $-t$, the contributions to the form-factor integral are concentrated at moderate-to-high x, where the valence quarks dominate. Therefore, the A_{LL} asymmetry contains direct information on $\Delta u(x)/u(x)$ in the valence region. We propose to investigate this in the present experiment, up to $-t = 6.4$ $(\mathrm{GeV}/c)^2$.

Obtaining this kind of information is one of the key physics elements justifying the 12 GeV upgrade of JLab. From the correspondence between RCS and electron scattering form factors, there is expected to be a close relationship between R_T/R_V and F_2/F_1 [9]. The measurements of G_E^p at JLab [4, 5] have shown that F_2/F_1 falls as $1/\sqrt{-t}$ rather than as $1/t$, the latter being predicted by pQCD. It will be an important check on the theoretical interpretation of F_2/F_1 to see if R_T/R_V behaves in a similar way.

2.5 Relativistic constituent quark model for RCS

The relativistic constituent quark model developed by G. A. Miller [15] addresses the question of what is the dominant reaction mechanism that allows the proton to accommodate the large momentum transfer in exclusive reactions like elastic electron and photon scattering. This model has been successful in describing the electromagnetic nucleon form factors [23]. Unlike the handbag calculations within the GPD approach [8, 9], Miller's model does not neglect quark and hadron helicity flip. The model starts with a wave function for three relativistic constituent quarks:

$$\Psi(p_i) = u(p_1)u(p_2)u(p_3)\psi(p_1, p_2, p_3),$$

where p_i represents space, spin, and isospin indices. It evaluates the wave function in the light cone variables and the calculations are relativistic. They obey gauge invariance, parity conservation, and time reversal invariance. They include quark mass effects and proton helicity flip. Due to lower components of Dirac spinors, where the quark spin is opposite to that of the proton, quark orbital angular momentum appears. The resulting predictions for the polarization observables A_{LL} and K_{LL} and the cross section are shown in Fig. 5 and Fig. 6, together with data from the E99-114 experiment. The most striking consequence of Miller's results is a big difference between A_{LL} and K_{LL} at large scattering angles, which we can test experimentally.

2.6 Polarization in QED Compton process

It is instructive to evaluate polarization effects in the QED process $e\gamma \to e\gamma$. The Klein-Nishina process is an example that is fully calculable and which plays a major role in RCS,

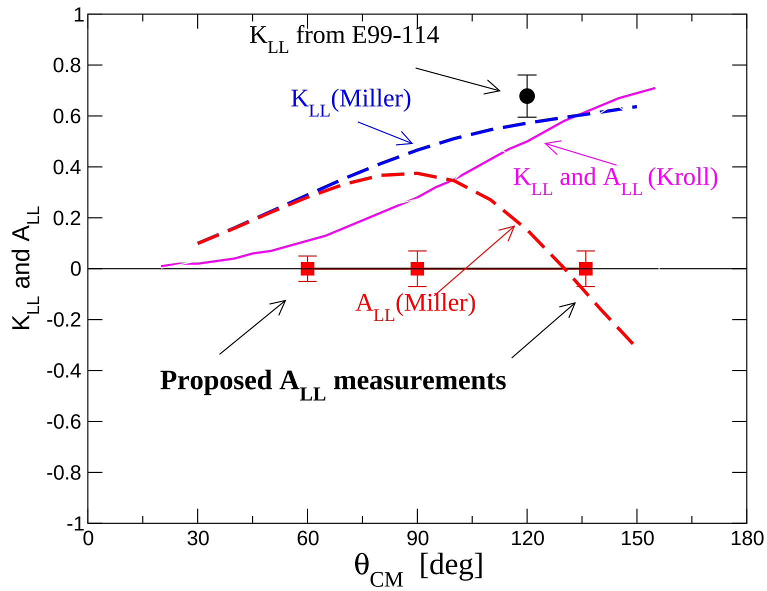

Figure 5: Predictions for A_{LL} in the GPD approach of Ref. [9] and CQM of Ref. [15] along with the data on $K_{LL}$from E99-114 and the expected precision of the proposed measurements.

when the handbag diagram dominates. It is useful to evaluate polarization observables for different ratios of the electron mass to the photon energy.

Polarization observables in QED are given in invariant variables as [24] :

$$A_{LL}^{KN} = \left[-\frac{s-m^2}{u-m^2} + \frac{u-m^2}{s-m^2} - \frac{2m^2t^2(s-u)}{(s-m^2)^2(u-m^2)^2}\right] / \left[-\frac{s-m^2}{u-m^2} - \frac{u-m^2}{s-m^2} + \frac{4m^2t(m^4-su)}{(s-m^2)^2(u-m^2)^2}\right]$$

$$K_{LL}^{KN} = \left[-\frac{s-m^2}{u-m^2} + \frac{u-m^2}{s-m^2} - \frac{4m^2t^2(m^4-su)}{(s-m^2)^3(u-m^2)^2}\right] / \left[-\frac{s-m^2}{u-m^2} - \frac{u-m^2}{s-m^2} + \frac{4m^2t(m^4-su)}{(s-m^2)^2(u-m^2)^2}\right]$$

Fig. 7 shows the A_{LL}^{KN} and K_{LL}^{KN} for different energies of the incident photon as a function of the scattering angle in the *lab*. At low t/s and for $m/E_\gamma << 1$ the difference between K_{LL} and A_{LL} vanishes. At $\theta_{lab} = \pi/2$ the observable A_{LL}=0. In the limit $m/E_\gamma \to 0$ A_{LL}=K_{LL} for all values of θ_γ not equal to 180°. At $\theta_\gamma = 180°$ the value of $A_{LL} \approx -K_{LL}$. If we now look at Miller's calculation (see Figure 5) which has $m/E_\gamma \sim 1/10$ and $\theta_{lab} \approx 90°$ (our kinematics labeled P2, see Table 4.1) the difference between $K_{LL}$and $A_{LL}$is about 0.7.

2.7 Additional Remarks

It is important to realize that the issues posed at the start of this section are not limited to the RCS reaction. Indeed, they are questions that need to be addressed by all studies of the proton using exclusive reactions in the hard scattering regime. The old paradigm for

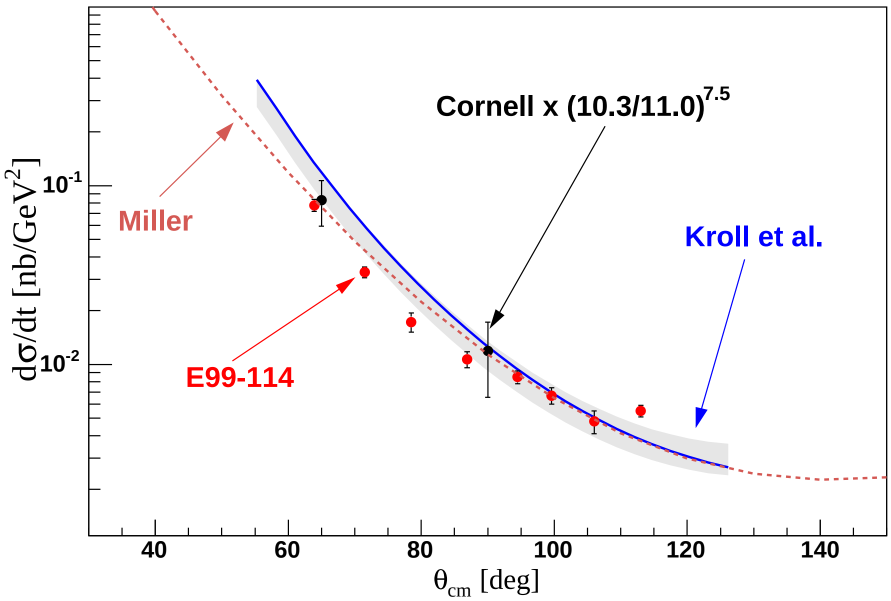

Figure 6: Cross section of RCS process at s = 11 (GeV/c)^2 from E99-114 and Cornell[25] experiments (scaled to the same CM energy) and results of calculations in the GPD approach (Kroll) and from a CQM (Miller).

addressing these questions was the pQCD mechanism and the distribution amplitudes. It is quite likely that the new paradigm will be the handbag mechanism and GPD's. In any case, the reaction mechanism needs to be tested, not only over a wide range of kinematic variables but also over a wide range of different reactions. Of these, RCS offers the best possibility to test the mechanism free of complications from additional hadrons. The CQM was quite successful in its description of many observables of the hadronic structure and generates a useful and intuitive picture of the hadron. The proposed test presents a unique case where predictions of the CQM and QCD–based theory are qualitatively different.

2.8 Theory Community Interest

During the preparation of this proposal, we contacted several theorists to gauge interest in a measurement of the initial state helicity correlation in WACS. The response was uniformly positive. We provide some of their feedback for context.

I think it is very interesting to measure A_{LL}. It will be either close to or far from K_{LL}. Either result would have important implications for understanding quark orbital angular mo-

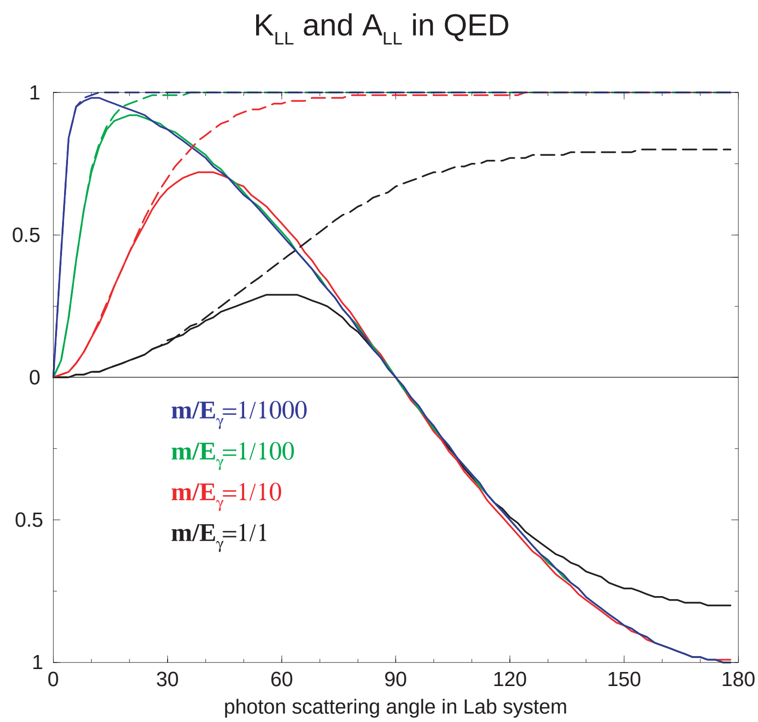

Figure 7: Klein-Nishina polarization observables A_{LL} and K_{LL}, shown by solid lines and dashed lines respectively, for different ratios of the electron mass to the photon energy as a function of the scattering angle in the lab system.

mentum in the proton. **Jerry Miller**

I am happy to learn that there is interest in RCS and am willing to support any activity of measuring A_{LL}. It is difficult to understand why there is still a lot of activity on DVCS at Jlab but not for RCS. **Peter Kroll**

The WACS polarization measurements on the proton will be of very help for developing the theory, since they are typically calculated with the same or slightly extended nonperturbative input as the unpolarized cross section. The physics situation has never been fully clarified. There may not be as much theoretical activity as a few years ago, which is not for lack of interest but due to the somewhat dormant situation regarding new data. **Markus Diehl**

A_{LL} can help determine how to estimate the unknown well defined nonperturbative quantities needed for modeling. **Nikolay Kivel**

2.9 Summary of Physics Goals

We propose measurements of the spin correlation asymmetry A_{LL} at an incident photon energy of 4.3 GeV, s=9 (GeV/c)^2, at two scattering angles; at $\theta_\gamma^{cm} = 70°$ corresponding to $-t$=2.4 (GeV/c)^2 and at $\theta_\gamma^{cm} = 140°$ corresponding to $-t$=6.4 (GeV/c)^2. The specific physics goals are as follows:

1. To make a measurement of A_{LL} at large s, t and u where applicability and limitations of GPD based calculations are under control. A high precision measurement will support the surprising result from Hall A for K_{LL}[6].

2. To provide a test that can expose, in an unambiguous way, how the RCS reaction proceeds: either via the interaction of photons with a current quark or, with a constituent quark.

3. To determine the form factor ratio R_A/R_V from the measurement of A_{LL} and correlate this ratio with the corresponding values of F_2/F_1 determined from elastic electron scattering.

The overall statistical precision with which we will address these physics goals will be discussed in Sec. 5.

3 Experimental Setup

The proposed experiment will study the scattering of polarized photons from a polarized hydrogen target, as illustrated in Fig. 8. The scattered photon will be detected by the Neutral Particle Spectrometer (NPS) installed at a distance to match the acceptance of the HMS, which will be used to detect the recoiling proton.

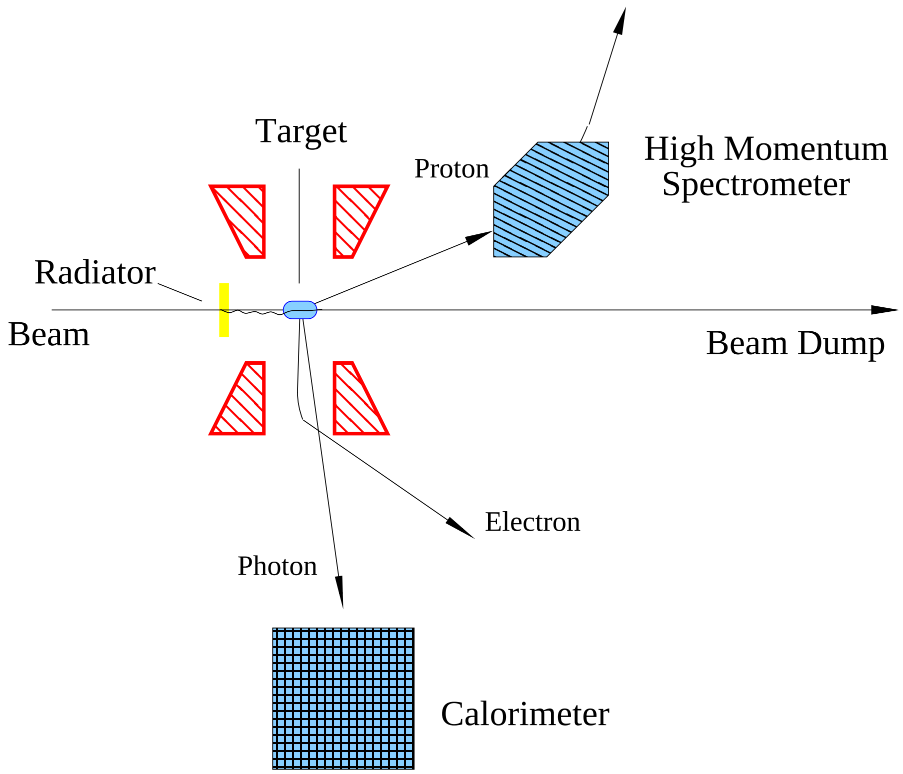

Figure 8: Schematic of the experimental setup. The target is longitudinally polarized (along the beam). The scattered photon is detected by NPS and the recoil proton is detected by the HMS. Teh scattered electron in the mixed photon-electron beam is deflected by the polarized target magnet.

We assume an incident electron beam of 4.4 GeV with intensity of 90 nA and 80% polarization. Such currents and polarizations have already been delivered using the strained GaAs source at Jefferson Lab before. The target will be a longitudinally polarized proton, which is the so called UVA polarized target, operating in a 5 Tesla field pointing to the longitudinal direction (along the beam line). Since the target field will deflect the charged particle sufficiently, we do not have to use a sweep magnet for the NPS.

With this beam intensity on UVA polarized target, a average NH_3 polarization of 75% have been achieved in several experiments, i.e. RSS, SANE experiments in Hall C, G2P and GEP experiments in Hall A. The beam polarization will be measured to a systematic uncertainty of 2% with the Hall C Möller polarimeter. The large cross section and helicity asymmetry for π^0 photoproduction, as determined from E99-114, will provide a monitor of the electron beam polarization continuously during data taking at fixed kinematic conditions with large θ_γ^{cm}.

3.1 The Polarized Hydrogen Target and the Radiator

In this experiment we will use the University of Virginia polarized target, which has been successfully used in E143/E155/E155x experiments at SLAC and E93-026, E01-006, E07-003, E08-007 and E08-027 at JLab. E08-007 and E08-027 used a different coil from Hall B, which is very similar to the original one except with larger penning. See Fig. 9 for a cross section view. We will polarized the target in longitudinal direction.

This target operates on the principle of Dynamic Nuclear Polarization (DNP). The low temperature (1 K°), high magnetic field (5 T) natural polarization of solid materials (ammonia, lithium hydrides) is enhanced by microwave pumping. The polarized target assembly contains two 3–cm–long target cells that can be selected individually by remote control to be located in the uniform field region of a superconducting Helmholtz pair. They are also 2 other target cells which are available for calibration target like carbon foil or CH_2. The permeable target cells are immersed in a vessel filled with liquid helium and maintained at 1 K by using a high power evaporation refrigerator. The magnet coils have a 55° conical shaped aperture along the axis and a 38° wedge shaped aperture along the vertically oriented midplane.

The target material, during the experiment, will be exposed to 140 GHz microwaves to drive the hyperfine transition which aligns the nucleon spins. The DNP technique produces proton polarizations of up to 95% in the NH_3 target. The heating of the target by the beam causes an initial drop of a few percent in the polarization. Then the polarization slowly decreases due to radiation damage. Most of the radiation damage is repaired by annealing the target at about 80 K, until the accumulated dose reaches $> 2 \times 10^{17}$ electrons, at which point the material needs to be changed. Due to limitations in the heat removal by the refrigerator, the luminosity (considering only the polarized material in the uniform field region) is limited to 85×10^{33} cm^{-2} Hz. As part of the program to minimize the sources of systematic errors, the target polarization direction will be reversed after each anneal by adjusting the microwave frequency.

A radiator will be mounted on the liquid nitrogen shield about 10 inches upstream of the target magnet center. The short distance between the target and radiator helps to avoid background produced from plastic target wall and downstream beam line. The separation of the events produced in the radiator is of order 5 cm (in the worst case) in the spectrometer y_{tg} coordinate, which is comfortably large compared to the y_{tg} resolution of 0.3 cm. We are going to use a copper radiator with thickness of 0.86 mm, which is 6% radiation length. Pair

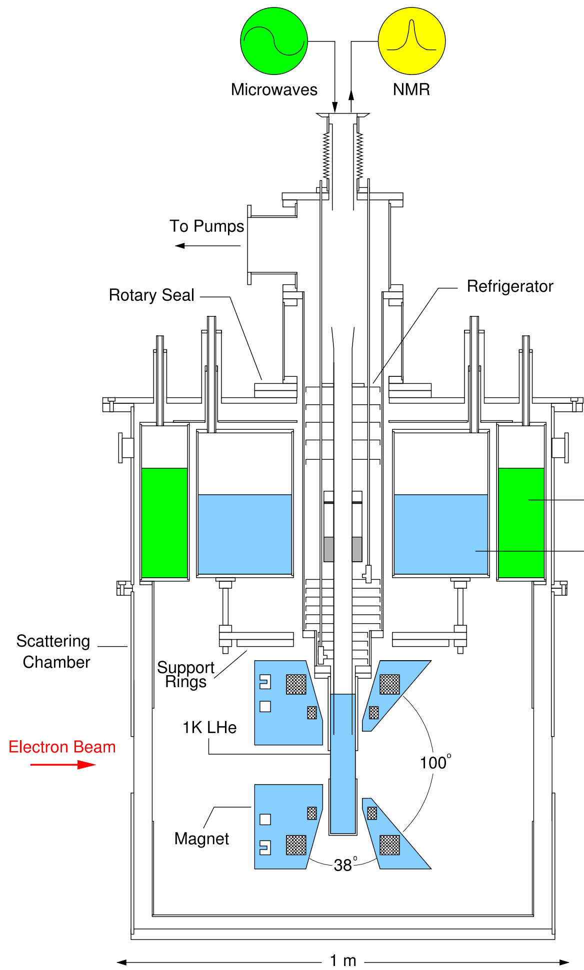

Figure 9: Cross section view of the polarized target.

production in the radiator will add 5.4% to the heat load of the refrigerator, so that the average beam current should be reduced by 5.4% yielding a useful luminosity of 80×10^{33} cm^{-2} Hz.

The polarized target magnet will deflect outgoing charged particles in both vertical and horizontal direction, which greatly improves the selection of the elastically scattered photons from the elastically scattered electrons at the calorimeter. The RCS experiment, E99-114, installed a sweep magnet between the target and the calorimeter to achieve similar result, but in their case the electrons were bent in the horizontal plane. Simulation shows that bending the charged particle (mainly electrons) in vertical will earn a better signal to background ratio since it allows to cut the uniform like background in both horizontal and vertical position.

3.2 The Photon Detector

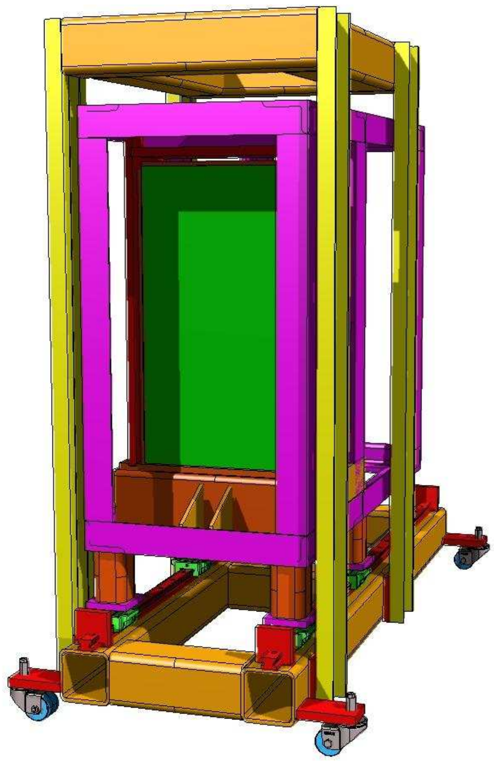

Figure 10: The front view of the Neutral Particle Spectrometer (NPS).

Members of this collaboration are participating in the construction of the Neutral Particle Spectrometer (NPS) for several future Hall C experiments, for example, E12-13-010, E12-13-007 and unpolarized future WACS experiments. The sensitive region of this calorimeter is 30 (horizontal) x 36 (vertical) inches, sitting on a frame which allows to move around. At Current design, the position resolution of the NPS is 3 mm and the energy resolution $\sigma_E/\sqrt{E}$ is better than 3%. Fig. 10 shows the front view of this calorimeter and its support structure.

We plan to place NPS in three locations. The forward angle position 22° (in the lab) serves two purposes: first to allow the calibration with elastically scattered electrons and also for production data taking at $\theta_{cm} = 60°$. The second position 37° is for production at $\theta_{cm} = 90°$. This is the most important location since 90 degrees in the CM frame is the most simple and clean scattering and also we want to compare the our A_{LL} to the K_{LL} at this point from

E07-002 and A_{LL}. The GPD predict that A_{LL}should not be different from K_{LL}while Miller's prediction predict a huge difference at large center of mass angle (See Fig 5). We should be able to see the difference at this point if there is true different between them. The third position is 78° in the lab, which is for production running at $\theta_{cm} = 136°$. The spectrometer angle of the HMS, which detects the protons, will be adjusted for each kinematics to match the photon scattering angle. The distance from the target to the calorimeter is chosen to insure an adequate angular coverage of the calorimeter to match HMS.

3.3 Proton Polarization in the Target

Polarization of the target will be measured by NMR with an absolute accuracy at the level of 1.5%. The P1 kinematics (see Table 4.1) will provide an opportunity for the independent determination of the proton polarization. In the P1 kinematics, scattered electrons will be deflected in the target by 1.7 degrees in the vertical direction, which leads to a vertical displacement of 23 cm at the front face of the calorimeter. For elastic electron proton scattering the beam–target asymmetry can be calculated from the following expression [27, 28]:

$$A^{ep} = \frac{2\sqrt{\tau(1+\tau)}\,\tan\frac{\theta}{2}}{g^2 + \tau\epsilon^{-1}} \cdot (g\,\sin\phi + \sqrt{\tau}\,\cos\phi) \tag{8}$$

where $g = G_E^p/G_M^p$ is the ratio of the proton form factors, θ is the scattering angle, $\tau = Q^2/4M_p^2$, (M_p is the proton mass), and $Q^2 = 4E_iE_f\sin^2\frac{\theta}{2}$, $E_{i(f)}$ is the initial (final) electron energy, $\epsilon^{-1} = 1 + 2(1+\tau)\tan^2\frac{\theta}{2}$ and $\sin\phi = \cos\frac{\theta}{2}/\sqrt{(1+E_i/M_p)(2+E_i/M_p)\sin^2\frac{\theta}{2}}$. This expression explicitly takes into consideration that the polarization axis is along the beam direction and in the scattering (horizontal) plane.

For $\theta_\gamma^{cm} = 60°$, $A = 0.45$. Through its measurement the product of the beam and the target polarization will be determined with a statistical accuracy of 0.02. This will provide an additional monitor of the beam and target polarization averaged over the duration of the data taking.

4 Proposed Measurements

An 80% longitudinally polarized electron beam with current of 90 nA at energy of 4.4 GeV will be used in the proposed experiment. A copper radiator with the thickness of 0.86 mm (6% radiation length) will be installed 10 inches upstream of the 3 cm NH_3 target, inside the scattering chamber. The circular polarization of the bremsstrahlung photon drops quickly as the photon energy decreasing. Their relationship is described by Eq. 9:

$$\frac{pol_\gamma}{pol_e} = \frac{4y - y^2}{4 - 4y + 3y^2}\,, \tag{9}$$

where $y = \frac{E_\gamma}{E_e}$ is the fraction of the photon energy to the electron beam energy.

We optimize the detector acceptance to pick those photons carry 80% to 95% of the incident electron energy. For such bremsstrahlung photons, the average circular polarization is about 97.6% of the polarization of the electrons. We will use HMS to detect the recoil proton in Hall C. The scattered photon will be detected by the future Neutral Particle Spectrometer(NPS).

4.1 The Kinematics

Table 4.1 shows the kinematics parameters of the proposed experiment. The central momentum of the proton spectrometer is determined through a Geant4 simulation and optimized for the maximum acceptance for incident photon energy from 80% to 95% of the electron beam energy. The distance of the front face of NPS to the target center (L) and its vertical offset (H) are also optimized for maximum RCS acceptance through the Gean4 simulation. The overlap of the acceptances of the photon and proton arms will be chosen in a way such that the angular acceptance is defined by the proton arm. Because the target field also bend the outgoing proton, those protons detected by HMS have an out-of-plane-angle offset. This also cause the outgoing photon have a opposite out-of-plane-angle offset. Therefore we have to shift the photon arm vertically by some height to balance it. These heights are listed as H in Table 4.1. For details of the kinematics, please refer to Fig. 11, Fig. 12 and Fig. 13.

4.2 Backgrounds

There are several sources of physics background in this measurement. The electrons, which lose energy while passing through the radiator and the target, can scatter elastically from the protons in the target. In this experiment the field of the polarized target magnet will provide sufficient deflection, we do not need to worry about them.

Another source is the quasireal photons from $ep\gamma$ event, $\mathrm{H}(e, p\gamma)e'$. Although the scattered electron is not detected, applying the $\gamma - p$ elastic kinematic correlation cuts, especially

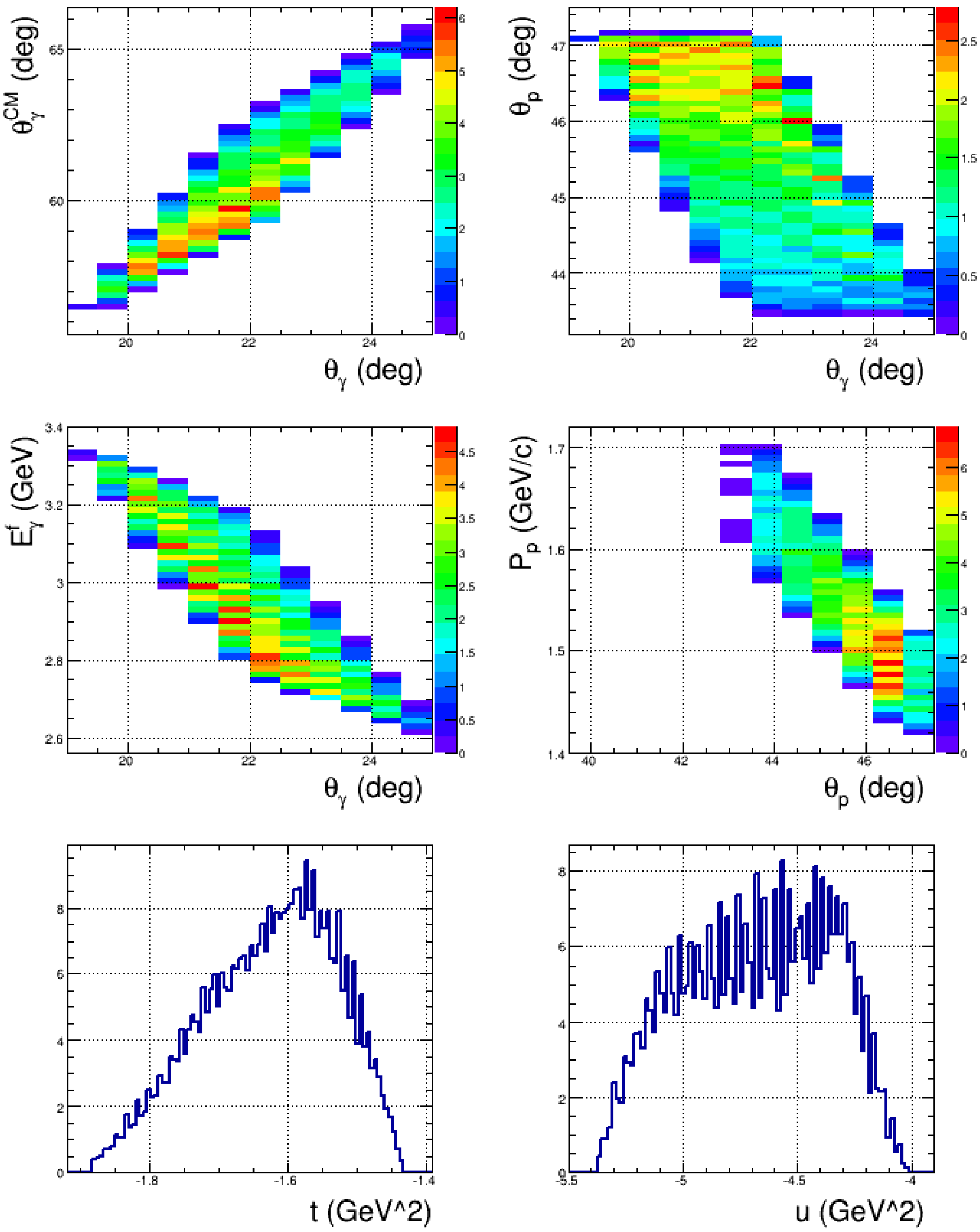

Figure 11: The kinematics coverage for P1.

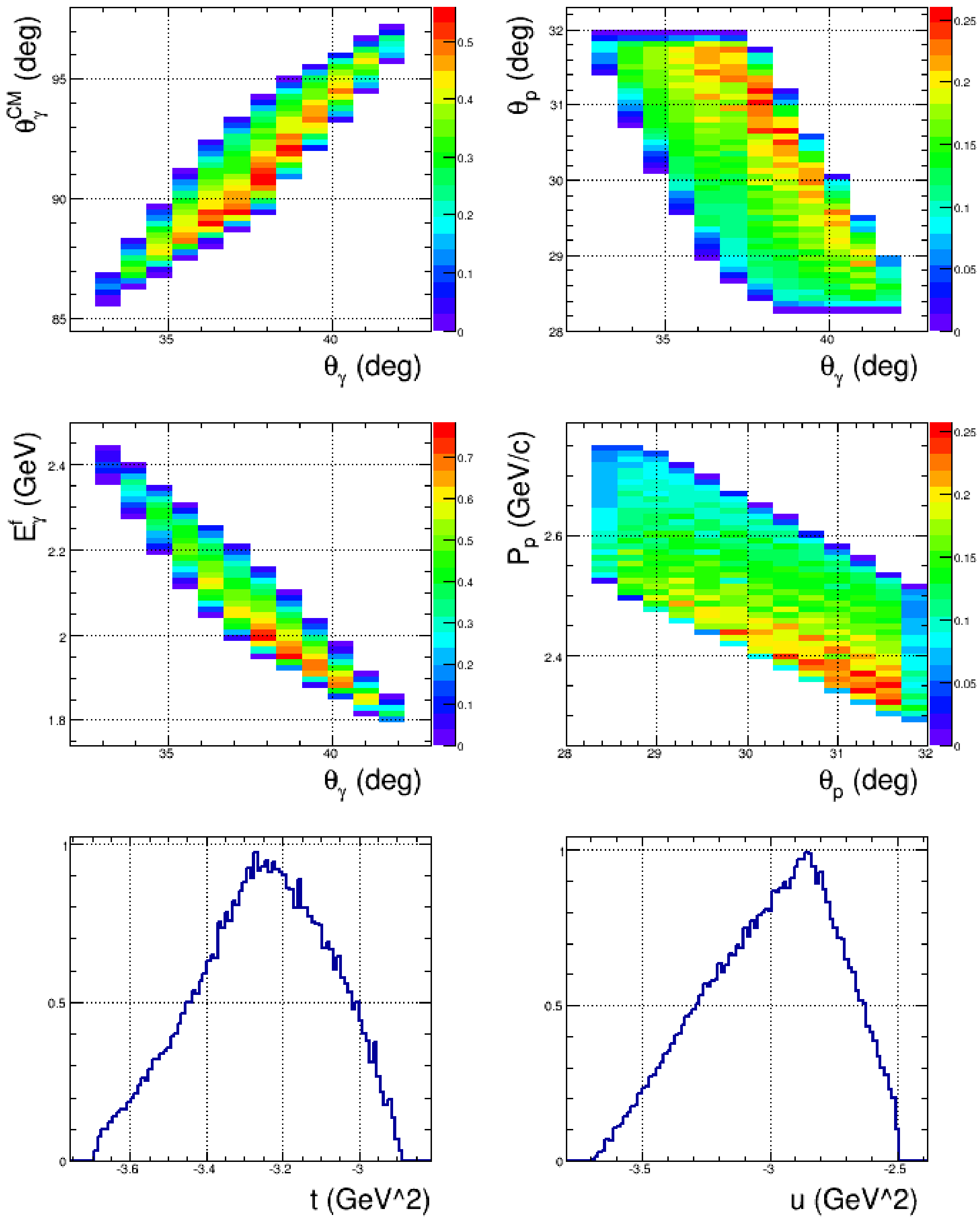

Figure 12: The kinematics coverage for P2.

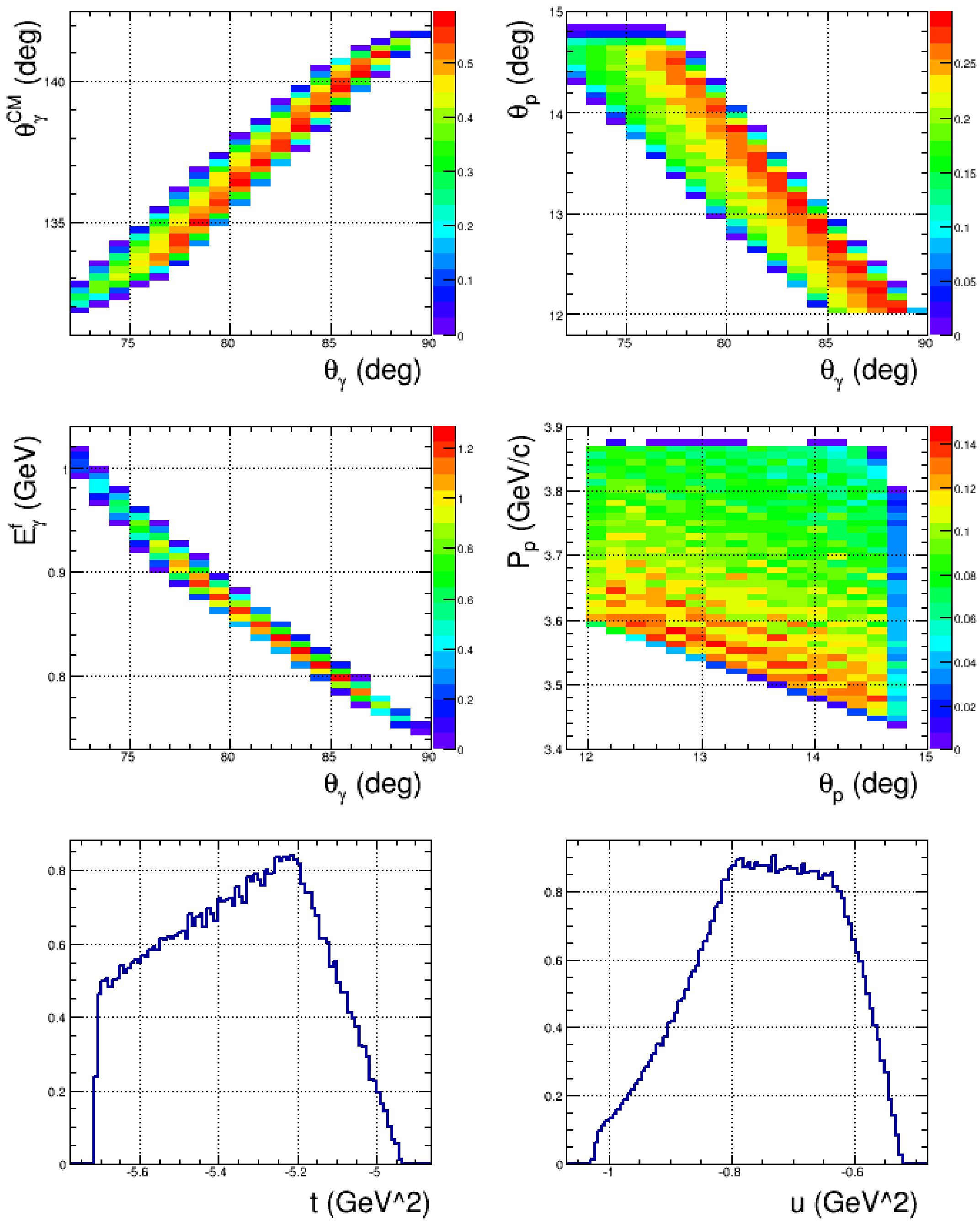

Figure 13: The kinematics coverage for P3.

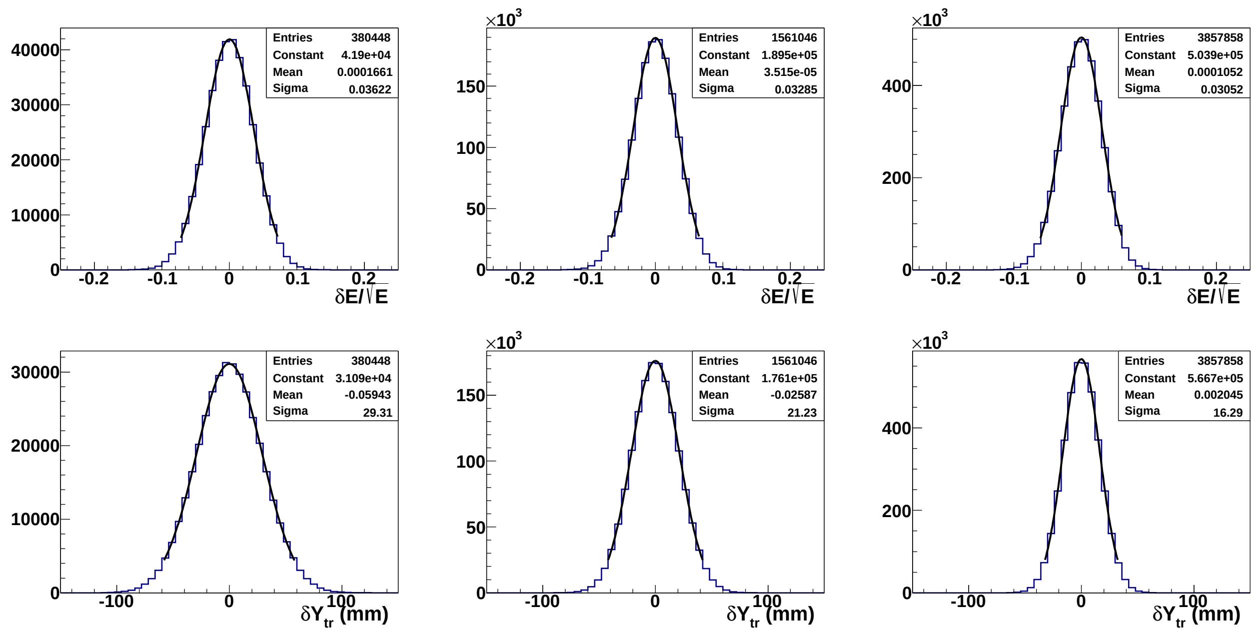

Figure 14: RCS correlation cuts of δE and δY for kinematics P1(left) and P2(center) and P3(right), where δE (top) is the difference between measured photon energy in the photon arm and the inferred photon energy, inferred by the measured proton in the proton arm, and δY(bottom) is the difference between measured photon horizontal position and the inferred photon horizontal position, in the transportation frame. A gaussian fit (black curve) is also plot on top of each histogram, with their fitted parameters labeled in the up-right corner in each panel. A 2-σ cut will be used in the data analysis to select good RCS events.

kin. P#	t, $(\mathrm{GeV}/c)^2$	θ_γ^{lab}, degree	θ_γ^{cm}, degree	θ_p^{lab}, degree	E_γ^{lab}, GeV	p_p, GeV/c	L, cm	H, cm
P1	-1.7	22	60	45	2.87	1.56	785	41.2
P2	-3.3	37	90	30	2.00	2.52	445	21.5
P3	-5.4	78	136	13	0.88	3.55	245	10.0

Table 1: The kinematics parameters of the proposed measurements at $s = 8$ $(\mathrm{GeV}/c)^2$.

the δE, δY and δX cuts (see Fig. 14 for details) will remove most of them. δE is the difference between measured photon energy in the photon arm and the inferred photon energy, inferred by the measured proton in the proton arm. $\delta Y(X)$ is the difference between measured photon horizontal(vertical) position and the inferred photon horizontal(vertical) position, in the transportation coordinate system. (The transportation coordinate is frequently used to define the acceptance and optics for in small acceptance spectrometer like HMS and HRS. In this coordinate system, z axis is the central ray, which line up with the spectrometer angle; x axis is vertical down and y axis is horizontal left when looking downstream.) According to our simulated result, $ep\gamma$ events drop rapidly as the scattering angle increasing. The ratio of $ep\gamma$ events to RCS events under the $2-\sigma$ cut is about 0.14, 0.08 and 0.03 for kinematics P1, P2 and P3, respectively. Our simulated $ep\gamma$ results match the exist E99-114 experiment pretty well, which states that the $ep\gamma$ contribution is about 11%-15% [37]. Nevertheless, these background can be analysis and subtracted in the data analysis. In this proposed measurement, since NPS have much better position and energy resolution while HMS has similar angular and position resolution as HRS, the $ep\gamma$ contribution will definitely be smaller.

The primary background come from neutral pion photoproduction from the protons in the target. It can be separated only on a statistical level by using a difference in the shapes of the distribution of RCS and $\mathrm{H}(\gamma, \pi^0)$ events. Fig. 15 shows the simulated δY and δX distribution, in the transportation coordinate system, for the proposed kinematics. This background leads to a large dilution factor, which affects the statistical accuracy of the measurements. The pion can also be produced from bound protons in nitrogen. Motion of the nucleons in nuclei, and FSI, reduce dramatically the dilution of RCS events. The nuclear pion process was investigated by using E99-114 data obtained from an aluminum target. We found that at conditions similar to those proposed here, pions produced from nuclei increase the dilution factor by less than 10%.

4.3 Signal Extraction

To reduce uncertainty in the extracted real Compton events it is possible to use a boosted decision tree [32, 33, 34, 35] with multiple discriminating variables. A decision tree is a binary tree structure classifier which organizes the data into regions and sorts event by event. The

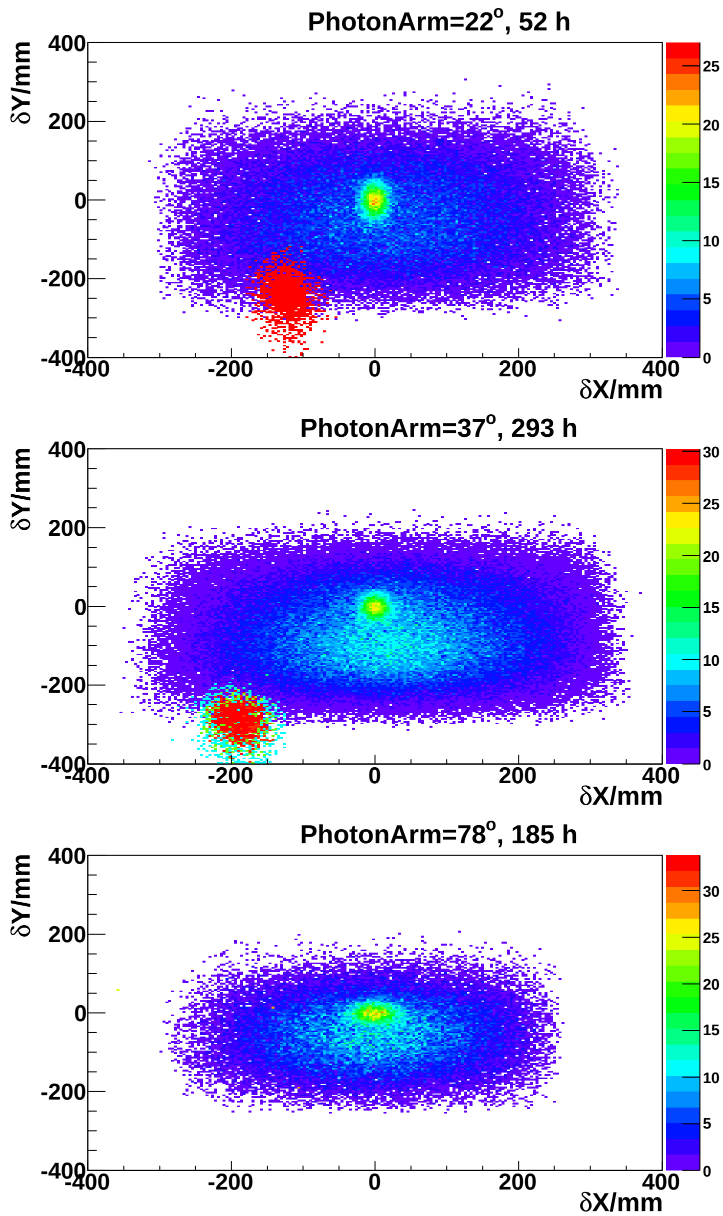

Figure 15: The δY and δX distribution, in the transportation coordinate system, after applying δE cut for RCS events and backgrounds for kinematics P1(top), P2(middle) and P3(bottom). The RCS events located at (0,0) and $e-p$ elastic events are deflected to negative δY and δX. The pi^0 backgrounds are evenly distributed everywhere. The statistics present here are corresponding to the requested beam time.

decision tree algorithm is able to split the phase space into a large number of hypercubes, each of which is identified as either signal or background. The boosting [36] performs best if applied to tree classiers that, taken individually, have not much classification power. Using a small set of input variables with weak classification power the uncertainty in the extracted counts can greatly be reduced.

As an example for separation of the RCS events from the pion background we use the discriminating variables δY, δX, and δP. The Monte Carlo is well tuned to the expect resolution of the detection system so that reconstruction of these variables is expected to be within a realistic range in the simulation. The decision tree is then trained and classification using simulated data of signal and the neutral pion background is obtained.

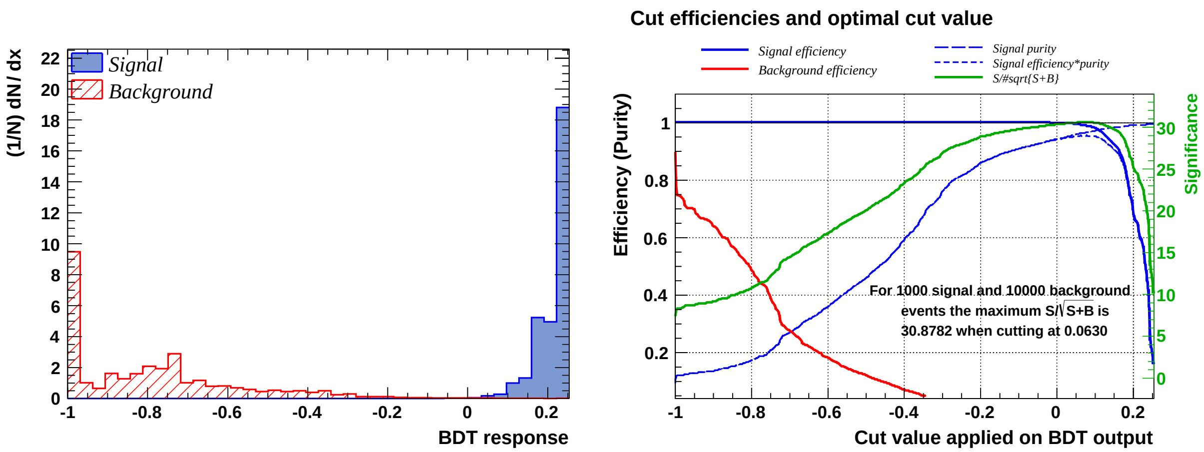

Figure 16: Results of analysis from the training of the boosted decision tree indicating (left) the response of the classifier and (right) the real Compton signal resolving efficiency.

Fig. 16 shows the boosted decision tree output. The classifier response indicates that even with the three mentioned discriminating variable it is possible obtain greater then 98% signal when making a constraint on the BDT response to eliminate the pion background. The cut value applied on the BDT response is indicated on the right showing that only around 40 events from the pion background survive after the constraint is applied when there is an order of magnitude more background than the Compton signal.

4.4 Rates

The event rates are the products of the luminosity, the cross section, and the acceptances of the detectors, as well all other factors such as DAQ dead time and detection efficiency.

The rate, $N_{_{RCS}}$ can be calculated as:

$$N_{_{RCS}} = \frac{d\sigma}{dt}_{_{RCS}} \frac{(E^f_\gamma)^2}{\pi} d\Omega_{\gamma p} A_{\gamma p} F_\gamma \mathcal{L}_{e\vec{p}} \,, \tag{10}$$

where $\frac{d\sigma}{dt}_{_{RCS}}$ is the RCS cross section; the factor $\frac{(E^f_\gamma)^2}{\pi}$ is the Jacobian that convert dt to $dEd\Omega$; $d\Omega_{\gamma p}$ is the solid angle of the RCS events that expressed in photon detector; $A_{\gamma p}$ is the acceptance of RCS events in the given range of photon energy E^f_γ; F_γ is the number of photons per incident electron, $\mathcal{L}_{e\vec{p}} = 7.5 \cdot 10^{34}$ cm^{-2}Hz is the electron-proton polarized luminosity with the NH_3 target, including a correction for the extra heat load from the radiator.

E99-114 measured real compton scattering cross section at four electron beam energy of 2.342, 3.481, 4.620, and 5.759 GeV and θ^{cm}_γ in the range of $60° - 130°$. Table 2 shows their result for the average photon energy of 4.3 GeV. Also shown in the table is the dilution factor D, which is defined as the ratio of total to signal of interest: $D = (N_{\gamma,\pi^\circ} + N_{\gamma,\gamma})/N_{\gamma,\gamma}$ for the kinematically correlated photon-proton events.

The value of D is highly affected by the accuracies of angle and and position of the reconstructed proton, and also the energy and position resolution of the photon detector.

kin. 4#	θ^{lab}_γ, degree	t, (GeV/c)^2	θ^{cm}_γ, degree	D	$d\sigma/dt$, pb/(GeV/c)^2
4A	22	-2.03	63.6	2.13	496.
4B	26	-2.57	72.8	1.54	156.
4C	30	-3.09	81.1	1.67	72.
4D	35	-3.68	90.4	2.75	42.
4E	42	-4.39	101.5	2.80	29.
4F	50	-5.04	112.1	2.42	38.
4G	57	-5.48	119.9	2.83	46.
4H	66	-5.93	128.4	3.89	61.

Table 2: The RCS cross section at s = 9 (GeV/c)^2- 4 pass kinematics in E99-114.

To estimate the RCS differential cross section, we modifies J. Miller's model [31] to match the exist data from E99-114 [37]. compared to E99-114 result, Miller's RCS differential cross section model has about 10% deviation in 3-pass data and 30% deviation for 4-pass and 43% deviation for 5-pass data. And also, E99-114 did not cover our P3 kinematics point where $\theta^{cm}_\gamma$is 136 degrees. Of course we can do an extrapolated but the uncertainty of it could be large. Miller's model has a good constraint on the center of mass angle dependence and incident photon energy dependence. Therefore we use a 5th order polynomial function to scale Miller's model such that it will match the exist E99-114 data. For any given photon energy and θ_γ^{cm}, we will do a 2nd order interpolation to calculate the RCS differential cross section. With this modification we are able to do estimation for θ_γ^{cm}larger than 130 degrees where E99-114 did not cover. Fig. 17 shows the modified model together with E99-114 data points.

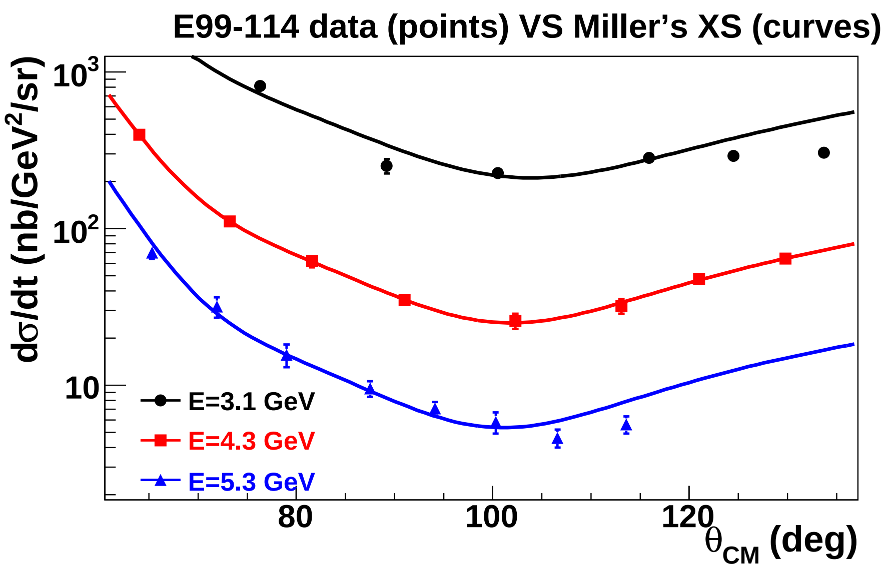

Figure 17: The RCS differential cross section. The solid curve is from modified Miller's model and solid points are the result from E99-114 [37].

To determine the angular acceptance, we developed a Geant4 simulation program. The whole target chamber with magnet coils and field are built together with detectors. We place detectors at the optimized locations and simulate RCS events, e-p elastic events and pi0 backgrounds. Finally we extract the acceptance for RCS photons in a 3-D space of energy, theta angle, and phi angle. We do the same thing to achieve the acceptance for electrons in NPS and protons in HMS.

For a 6% radiator, the photon flux can be calculated as:

$$F_\gamma = t_{rad}[\frac{4}{3}\ln(\frac{k_{max}}{k_{min}}) - \frac{4(k_{max} - k_{min})}{3E} + \frac{k_{max}^2 - k_{min}^2}{2E^2}], \tag{11}$$

where k_{max} and k_{min} are the upper and lower limit of the radiated photon energies, E is the electron beam energy and t_{rad} is the thickness of the radiator in the unit of radiation length.

Our event rates are integrated over the 3-D space of energy, theta angle, and phi angle using Eq. 10. Table 3 shows the rates and dilution factors D, which is the fraction of total to signal. The expected δX distributions for RCS signal and backgrounds after applying those cuts shown in Fig. 14, are present in Fig. 18. The pure RCS signal is red curves, with a gaussian fit (pink) on top of it. The fitted parameters are labeled in the up-right coroner of each panel. The e-p elastic events also plot in the figure but almost nothing survive after the 3-σ δE and δY cuts. The statistics here represent for 41, 445 and 240 hours of data taking for kinematics P1, P2 and P3, respectively.

kin. P#	θ_γ^{lab}, degree	θ_γ^{cm}, degree	RCS rate, Hz	D,	N_{RCS}, per hour
P1	22	60	0.01254	2.0	45.1
P2	37	90	0.00158	2.8	5.7
P3	78	136	0.00339	3.9	12.2

Table 3: The kinematic parameters and the expected counts.

4.5 Required Statistics

The statistics required for obtaining the specified accuracy of ΔA_{LL} can be calculated from

$$N_{RCS,required} = D/(P_e P_p f_{e\gamma} \Delta A_{LL})^2$$

where $P_e = 0.85$ is the electron beam polarization, $P_p = 0.75$ is the averaged proton polarization in the target, $f_{e\gamma} = 0.98$ is the ratio of the photon and the electron polarizations for the average $E_\gamma = 0.9E_e$. Table 4 presents the required statistics for a precision of $\Delta A_{LL} = 0.05$ for all kinematics points.

kinematic	P1	P2	P3
N_{RCS}, events	2333	1666	2261
ΔA_{LL}	0.05	0.07	0.07

Table 4: The statistics and expected precision in the proposed experiment.

4.6 Systematic Uncertainty

Table 5 shows a list of the scale dependent uncertainties contributing to the systematic error in A_{LL}. With careful uncertainty minimization in polarization the relative error in P can be less than or equal to 3.9%, as demonstrated in the recent E08-027/E08-007 experiment [38].

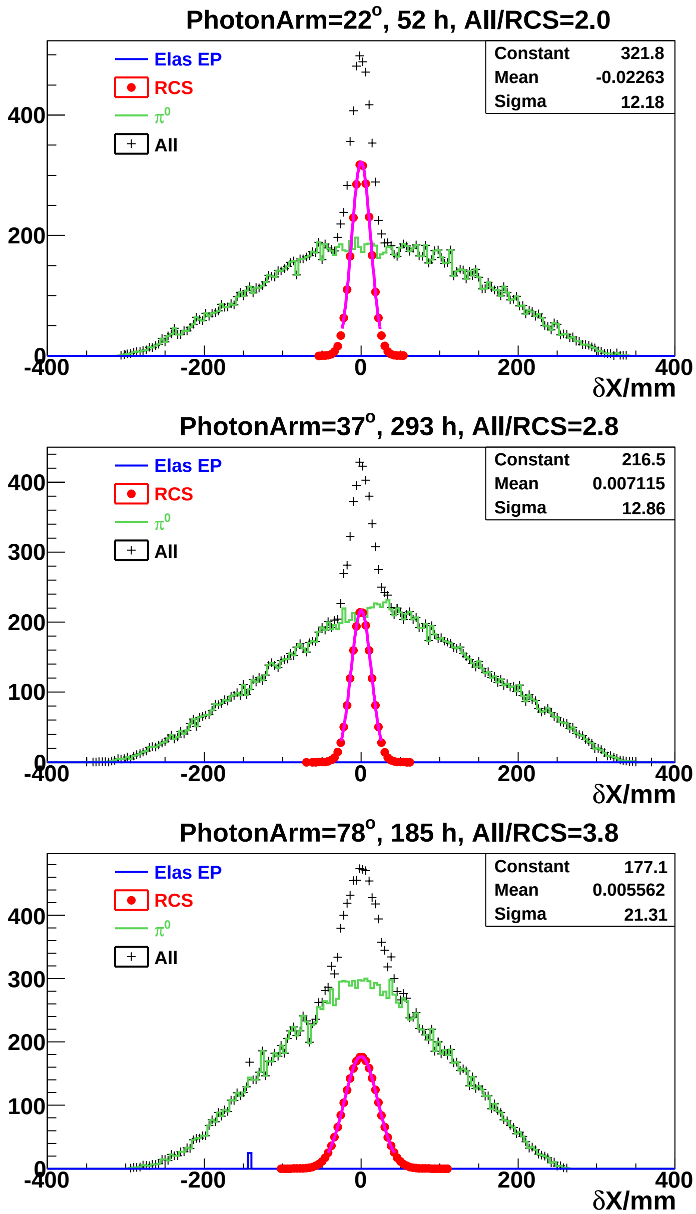

Figure 18: δX distributions after δE and δY cuts, for kinematics P1(top), P2(middle) and P3(bottom). The pure RCS signal is red curves, with a gaussian fit (pink) on top of it. The fitted parameters are labeled in the up-right coroner of each panel. The e-p elastic events also plot in the figure but almost nothing survive after δE and δY cuts. The total (RCS+π^0) are the black curves.

Source	Systematic
Polarimetry	5%
Packing fraction	3%
Trigger/Tracking efficiency	1.0%
Acceptance	0.5%
Charge Determination	1.0%
Detector resolution and efficiency	1.0%
Background subtraction	4.0%
Total	8%

Table 5: Estimates of the scale dependent contributions to the systematic error of A_{LL}.

The uncertainty in the packing fraction of the ammonia target contributes at a level of less than 3%.

Charge calibration and detector efficiencies are expected to be known better to 1%. Detector resolution and efficiency is also expect to contribute less than 1%.

The signal extraction error will be minimized using a multivariate techniques leading to only a few counts of background slipping into the final result. The systematic error on resolving the Compton signal is dependent on the background produced at that kinematic point. A larger background with smaller signal naturally results in a larger error. By considering a larger then expected background we can estimate the expected systematic error from a plausible analysis. Considering both π^0 and $ep\gamma$ background we expect less than a 4% background which is a estimate directly based on the Monte Carlo.

The primary sources of systematic error clearly come from polarimetry and background subtraction but the impact of time-dependent drifts in these quantities must be carefully controlled.

The asymmetry involves the ratio of counts, which leads to cancelation of several first order systematic effects. However, the fact that the two data sets will not be taken simultaneously leads to a sensitivity to time dependent variations which will be carefully monitored and suppressed. The systematic differences in the time dependent components of the integrated counts, we need to consider the effects from calibration, efficiency, acceptance, and luminosity between the two polarization states. However due to the quick change in beam polarity these effect have near negligible effect with respect to the scale dependent terms.

5 Expected Results and Beam Time Request

5.1 Expected Results

The purpose of this experiment is to measure the initial state helicity correlation asymmetry A_{LL} with a precision sufficient to obtain conclusive evidence on the dominance of the specific reaction mechanism. Another purpose is to determine the form factor ratio: R_A/R_V, which is also related to A_{LL}. We propose to obtain the statistical precision for A_{LL}, given in Table 4 and shown in Fig. 19. Using the handbag formalism to interpret the results of the A_{LL}, we will extract values for R_A/R_V.

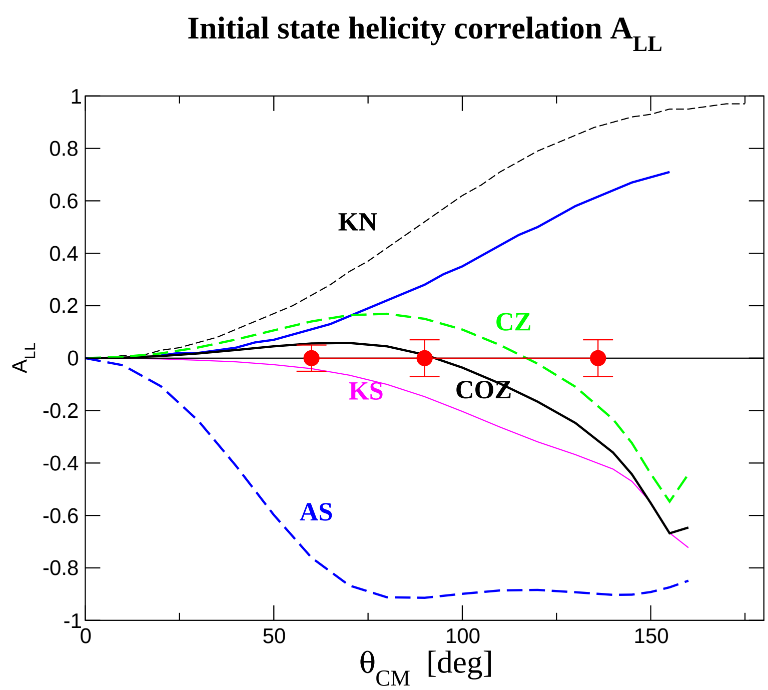

Figure 19: The initial state helicity correlation asymmetry A_{LL} in the RCS process with the expected precision of the proposed measurements shown as closed squares. The labels on the curves are as follows: CQM for the asymmetry in the constituent quark model[15]; the pQCD calculations[3] with AS for the asymptotic distribution amplitudes; with COZ for Chernyak-Ogloblin-Zhitnitsky [30]; GPD for calculations in the soft overlap approach[9]. The K_{LL} result[6] from E99-114 is also shown.

5.2 Beam Time Request

The proposed experiment will be done at one beam energy of 4.4 GeV with currents of 90 nA. The requested beam time summarized in Tables 6.

We require 8 hours to calibrate the calorimeter with $e - p$ elastics coincident events. Radiator will not be seen by the beam line during this procedure. To measure the packing fraction of the material in the target cell, we need 22 hours in total to do empty cell and carbon measurements. We need to measure the beam polarization with the Möller polarimetry every time the beam condition change. We estimate the frequency in the order of once every other day. It will take about 3 hours for each measurement. In total we requested 33 hours.

Also shown in Table 6 is a summary of the time required for configuration changes. It will take about 3 hours to perform each anneal of the target in order to restore the target polarization. We will need one anneal every 2 days in average, according to the latest experience in E08-007 and E08-027. In the worst case, we might need to change the target stick 3 time with fresh material. This changes will take about twelve hours to change the material and perform a new target polarization calibrations.

To change kinematics (move NPS and HMS), it will require about 6 hours for each change.

The total time requested is a combination of the required beam time and the overhead time. From experience running GEN, RSS, SANE, E08-007 and E08-027, we know that roughly one-half of the overhead can be performed during times when the accelerator is not delivering physics beam to the Halls. Thus, our total requested time is the sum of the beam time and one-half of the overhead time. The total request is 742 hours, or 31 days.

Kin. P#	Procedure	beam, nA	time hours
P1	RCS data taking	90	52
P2	RCS data taking	90	293
P3	RCS data taking	90	185
P1	NPS and HMS calibration	1000	8
P2	NPS and HMS calibration	1000	8
P3	NPS and HMS calibration	1000	8
	Packing Fraction	90	22
	Moller Measurements	200	33
	Beam Time		601
	Target Anneals		33
	Stick Changes		36
	kinematics change		12
	50% Overhead Time		60
	Total Requested Time		742

Table 6: The beam time request for the experiment.

6 Summary

We request 742 hours of beam time to measure the initial state helicity correlation asymmetry A_{LL} in RCS at s= 8 (GeV/c)^2 for θ_γ^{cm} = 60°, 90° and 136° with uncertainty of 0.05, 0.07 and 0.07, respectively. This experiment will take place in Hall C, utilizing a 4.4 GeV, 90 nA and 80% polarized electron beam, plus the UVA polarized target (longitudinally polarized), and HMS to detect protons, and NPS to detect scattered photons. This is a unique opportunity to study the initial state polarization effects in RCS.

Knowledge of the initial state helicity correlation asymmetry A_{LL} in RCS at these kinematics will allow a rigorous test of the reaction mechanism for exclusive reactions at high t, which is crucial for the understanding of nucleon structure.

Furthermore, it will be an extended measurement of the proton axial form factor R_A in RCS, which is the $1/x$ moment of the polarized parton distribution.

References

[1] S. J. Brodsky and G. Farrar, *Phys. Rev. Lett.* **31**, 1153 (1973).

[2] V. A. Matveev, R. M. Muradyan, and A. V. Tavkheldize, *Lett. Nuovo Cimento* **7**, 719 (1973).

[3] T. Brooks and L. Dixon, *Phys. Rev.* **D 62** 114021 (2000)

[4] M. Jones *et al.*, *Phys. Rev. Lett.* **84**, 1398 (2000).

[5] O. Gayou *et al.*, *Phys. Rev. Lett.* **88**, 092301 (2002).

[6] D. J. Hamilton *et al.* [Jefferson Lab Hall A Collaboration], arXiv:nucl-ex/0410001.

[7] A.V. Radyushkin, *Phys. Rev.* **D 58**, 114008 (1998).

[8] M. Diehl, T. Feldmann, R. Jakob, P. Kroll, *Eur. Phys. J.* **C 8**, 409 (1999).

[9] H. W. Huang, P. Kroll, T. Morii, *Eur. Phys. J.* **C 23**, 301 (2002), *Erratum ibid.*, **C 31**, 279 (2003); H. W. Huang, private communication.

[10] X. Ji, *Phys. Rev.* **D 55**, 7114 (1997), *Phys. Rev. Lett.* **78**, 610 (1997).

[11] A.V. Radyushkin, *Phys. Lett.* **B 380**, 417 (1996), *Phys. Rev.* **D 56**, 5524 (1997).

[12] N. Kivel and M. Vanderhaeghen, JHEP 1304 (2013) 029; arXiv:1212.0683.

[13] N. Kivel and M. Vanderhaeghen, arXiv:1312.5456 [hep-ph].

[14] M. Diehl, P. Kroll, *Eur. Phys. J.* **C 73**, 2397 (2013), arXiv:1302.4604.

[15] G. A. Miller, *Phys. Rev.* **C 69**, 052201(R) (2004).

[16] A. Nathan, R. Gilman and B. Wojtsekhowski, spokespersons, JLab experiment E07-002.

[17] G. P. Lepage and S. J. Brodsky, *Phys. Rev.* **D 22**, 2157 (1980).

[18] A. Radyushkin, arXive:hep-ph/0410276 and Dubna preprint JINR P2 10717.

[19] G. R. Farrar and H. Zhang, *Phys. Rev. Lett.* **65**, 1721 (1990), *Phys. Rev.* **D 42**, 3348 (1990).

[20] A. S. Kronfeld and B. Nizic, *Phys. Rev.* **D 44**, 3445 (1991); M. Vanderhaeghen, P. A. M. Guichon and J. Van de Wiele, *Nucl. Phys.* **A 622**, 144c (1997).

[21] K. Wijesooriya *et al.*, *Phys. Rev. C***66**, 034614 (2002).

[22] M. Diehl, T. Feldmann, R. Jakob and P. Kroll, *Eur. Phys. J.* **C 39**, 1 (2005) arXiv:hep-ph/0408173.

[23] G. A. Miller, *Phys. Rev.* **C 66**, 032201 (2002).

[24] M. Diehl, T. Feldmann, H. W. Huang and P. Kroll, Phys. Rev. D **67**, 037502 (2003) [arXiv:hep-ph/0212138].

[25] M. A. Shupe *et al.*, *Phys. Rev.* **D 19**, 1921 (1979).

[26] C. Perdrisat *et al.*, JLab experiment E01-109, 2001.

[27] N. Dombey, Rev. Mod. Phys. 41, 236 (1969).

[28] T. W. Donnelly and A. S. Raskin, Ann. Phys. (New York) 169, 247 (1986); 191, 81 (1989).

[29] Spin Asymmetries of the Nucleon Experiment, JLAB E-03-109, O.Rondon, Z.E. Meziani, and S. Choi, spokespersons.

[30] V. L. Chernyak A. A. Oglobin, and A. R. Zhitnitsky, *Z. Phys.* **C 42**, 569 (1989).

[31] G. Miller, Phys. Rev. C, 69, 052201.

[32] L. Breiman, J. Friedman, R. Olshen and C. Stone, “Classication and Regression Trees”, Wadsworth International Group, Belmont, California (1984).

[33] J. Friedman, T. Hastie, and R. Tibshirani, “Additive logistic regression: a statistical view of boosting”, Annals of Statistics 28 (2), 337-407 (2000).

[34] Y. Freund and R.E. Schapire, A short introduction to boosting, Journal of Japanese Society for Artificial Intelligence, 14(5), 771-780.

[35] J. Friedman, Recent Advances in Predictive (Machine) Learning, Proceedings of Phystat2003, Stanford University, (September 2003).

[36] R.E. Schapire, The boosting approach to machine learning: An overview, MSRI Workshop on Nonlinear Estimation and Classification, (2002).

[37] A. Danagoulian *et al.*, Phys. Rev. Lett, 98, 152001 (2007).

[38] D. Keller, Nucl. Inst. and Meth. A728 133-144 (2013)